



# DETECTION OF HF TOWARD PKS 1830–211, SEARCH FOR INTERSTELLAR $\text{H}_2\text{F}^+$ , AND LABORATORY STUDY OF $\text{H}_2\text{F}^+$ AND $\text{H}_2\text{Cl}^+$ DISSOCIATIVE RECOMBINATION

K. KAWAGUCHI<sup>1</sup>, S. MULLER<sup>2</sup>, J. H. BLACK<sup>2</sup>, T. AMANO<sup>3</sup>, F. MATSUSHIMA<sup>4</sup>, R. FUJIMORI<sup>5</sup>, Y. OKABAYASHI<sup>1</sup>, H. NAGAIRO<sup>1</sup>, Y. MIYAMOTO<sup>1</sup>, AND J. TANG<sup>1</sup>

<sup>1</sup> Graduate School of Natural Science and Technology, Okayama University, Okayama 700-8530, Japan

<sup>2</sup> Department of Earth and Space Sciences, Chalmers University of Technology, Onsala Space Observatory, SE-43992 Onsala, Sweden

<sup>3</sup> Department of Chemistry and Department of Physics and Astronomy, University of Waterloo, Waterloo, ON, N2L 3G1, Canada

<sup>4</sup> Department of Physics, Faculty of Science, University of Toyama, Toyama 930-8555, Japan

<sup>5</sup> Institute for Space-Earth Environmental Research, Nagoya University, Nagoya 464-8601, Japan

Received 2016 January 5; accepted 2016 March 13; published 2016 May 12

## ABSTRACT

We report extragalactic observations of two fluorine-bearing species, hydrogen fluoride (HF) and fluoronium ( $\text{H}_2\text{F}^+$ ), in the  $z = 0.89$  absorber in front of the lensed blazar PKS 1830–211 with the Atacama Large Millimeter/submillimeter Array. HF was detected toward both southwest and northeast images of the blazar, with column densities  $>3.4 \times 10^{14} \text{ cm}^{-2}$  and  $0.18 \times 10^{14} \text{ cm}^{-2}$ , respectively.  $\text{H}_2\text{F}^+$  was not detected, down to an upper limit ( $3\sigma$ ) of  $8.8 \times 10^{11} \text{ cm}^{-2}$  and an abundance ratio of  $[\text{H}_2\text{F}^+]/[\text{HF}] \leq 1/386$ . We also searched for  $\text{H}_2\text{F}^+$  toward the Galactic sources NGC 6334 I and W51C, and toward Galactic center clouds with the *Herschel* HIFI spectrometer.<sup>6</sup> The upper limit on the column density was derived to be  $2.5 \times 10^{11} \text{ cm}^{-2}$  in NGC 6334 I, which is  $1/68$  of that for  $\text{H}_2\text{Cl}^+$ . In contrast, the ortho transition of  $\text{H}_2\text{Cl}^+$  is detected toward PKS 1830–211. To understand the small abundance of interstellar  $\text{H}_2\text{F}^+$ , we carried out laboratory experiments to determine the rate constants for the ion–electron recombination reaction by infrared time-resolved spectroscopy. The constants determined are  $k_e(209 \text{ K}) = (1.1 \pm 0.3) \times 10^{-7} \text{ cm}^3 \text{ s}^{-1}$  and  $(0.46 \pm 0.05) \times 10^{-7} \text{ cm}^3 \text{ s}^{-1}$  for  $\text{H}_2\text{F}^+$  and  $\text{H}_2\text{Cl}^+$ , respectively. The difference in the dissociative recombination rates between  $\text{H}_2\text{F}^+$  and  $\text{H}_2\text{Cl}^+$  by a factor  $\sim 2$  and the cosmic abundance ratio  $[\text{F}]/[\text{Cl}] \approx 1/6$  are not enough to explain the much smaller abundance of  $\text{H}_2\text{F}^+$ . The difference in the formation mechanism of  $\text{H}_2\text{F}^+$  and  $\text{H}_2\text{Cl}^+$  in interstellar space would be a major factor in the small abundance of  $\text{H}_2\text{F}^+$ .

**Key words:** galaxies: individual (PKS 1830–211) – ISM: individual objects (W31C, NGC 6334 I) – ISM: molecules – methods: laboratory: molecular

## 1. INTRODUCTION

The hydrogen fluoride (HF) molecule was first detected in space by Neufeld et al. (1997) toward Sgr B2, using the *Infrared Space Observatory*. Later,  $\text{CF}^+$  was detected toward the Orion bar region (Neufeld et al. 2006), where the detection was driven by a theoretical study (Neufeld et al. 2005) of fluorine-bearing molecules in the interstellar medium. HF and  $\text{CF}^+$  are significant fluorine-bearing molecules in interstellar space, while AlF was detected in a circumstellar envelope by Cernicharo & Guélin (1987). Recently, HF was detected in many interstellar clouds with the Heterodyne Instrument for the Far-Infrared (HIFI) on board the *Herschel* Space Observatory (Neufeld et al. 2010; Phillips et al. 2010; Sonnentrucker et al. 2010, 2015; Monje et al. 2011a). HF was also detected in four nearby galaxies: in Mrk 231 (van der Werf et al. 2010, in emission) and Arp 220 (Rangwala et al. 2011) with the *Herschel* SPIRE-FTS, and in NGC 253 and NGC 4945 using HIFI (Monje et al. 2014). The detection of HF toward a high-redshift quasar at  $z = 2.56$  was reported by Monje et al. (2011b) using the Caltech Submillimeter Observatory. The observed abundance of HF in diffuse clouds was found to be consistent with theoretical predictions of Neufeld et al. (2005), Neufeld & Wolfire (2009), and Sonnentrucker et al. (2015), where in the latest report they carried out some updates of reaction data and also included grain surface chemistry.

In the present paper, we report the detection of HF in the  $z = 0.89$  molecular absorber toward PKS 1830–211 and searches for  $\text{H}_2\text{F}^+$  toward PKS 1830–211 and other Galactic sources.  $\text{H}_2\text{F}^+$  is isovalent with  $\text{H}_2\text{Cl}^+$  and isoelectronic to  $\text{H}_2\text{O}$ . In 2010, Lis et al. reported the detection of  $\text{H}_2\text{Cl}^+$  toward NGC 6334 I and Sgr B2 with HIFI. Recently,  $\text{H}_2\text{Cl}^+$  was also detected toward PKS 1830–211 (Muller et al. 2014a) with the Atacama Large Millimeter/submillimeter Array (ALMA). The existence of the related  $\text{H}_2\text{F}^+$  ion in interstellar clouds would be interesting from the viewpoint of halogen chemistry. A purely rotational spectroscopic study of  $\text{H}_2\text{F}^+$  was reported by Fujimori et al. (2011), who measured five rotational lines of  $\text{H}_2\text{F}^+$  in the ground state by using a submillimeter-wave spectrometer based on a backward-wave oscillator (BWO) at the University of Waterloo. Since the BWO measurement was limited in the frequency region below 775 GHz, higher frequency transitions were covered by a tunable far-infrared spectrometer at the University of Toyama (Amano et al. 2012), and seven lines were detected in the region 1305–1851 GHz. These spectroscopic studies made it possible to search for  $\text{H}_2\text{F}^+$  in interstellar space. However, the rotational transition frequencies from the lowest state are not accessible to ground-based telescopes because of atmospheric absorption. Therefore, observations were carried out toward the  $z = 0.89$  molecular-rich absorber in front of PKS 1830–211 (see, e.g., Muller et al. 2011) using the ALMA and toward Galactic sources with the *Herschel* Space Observatory.

The *Herschel* Space Observatory detected many new interstellar molecules and molecular ions. In particular,  $\text{H}_2\text{O}^+$  (Ossenkopf et al. 2010),  $\text{HCl}^+$  (De Luca et al. 2012),

<sup>6</sup> *Herschel* is an ESA space observatory with science instruments provided by European-led Principal Investigator consortia and with important participation from NASA.

$\text{H}_2\text{Cl}^+$  (Lis et al. 2010), and  $\text{ArH}^+$  (Schilke et al. 2014) were first detected in relatively low-density clouds with  $\text{H}_2$  density of less than  $10^3 \text{ cm}^{-3}$ . The proton affinity of HF (484  $\text{kJ mol}^{-1}$ ) is larger than that of  $\text{H}_2$  (422  $\text{kJ mol}^{-1}$ ), but smaller than those of CO (594  $\text{kJ mol}^{-1}$ ) and  $\text{N}_2$  (494  $\text{kJ mol}^{-1}$ ). Therefore, low-density clouds become potentially good candidates for searching for  $\text{H}_2\text{F}^+$ . Since  $\text{H}_2\text{F}^+$  has been thought to be produced through the reaction of  $\text{H}_3^+$  and HF,  $\text{H}_2\text{F}^+$  may be a direct proxy for  $\text{H}_3^+$  in diffuse clouds.

In spite of sensitive searches for  $\text{H}_2\text{F}^+$  in the present study, the ion is still not detected in space. Its abundance depends on production and/or depletion mechanisms. In diffuse clouds, the depletion is dominated by dissociative recombination reactions with electrons. Neufeld et al. (2005) and Neufeld & Wolfire (2009) estimated the rate constant  $k_e$  for the following dissociative recombination reactions in their chemical study of fluorine-bearing molecules:

$$\text{H}_2\text{F}^+ + e \rightarrow \text{HF} + \text{H}$$

$$k_e = 3.5 \times 10^{-7} (T/300 \text{ K})^{-0.5} \text{ cm}^3 \text{ s}^{-1} \quad (1)$$

$$\text{H}_2\text{F}^+ + e \rightarrow \text{F} + \text{products}$$

$$k_e = 3.5 \times 10^{-7} (T/300 \text{ K})^{-0.5} \text{ cm}^3 \text{ s}^{-1}. \quad (2)$$

Various kinds of experimental methods have been reported for determining the recombination rate constants, as summarized by Plašil et al. (2002) and Geppert & Larsson (2008). Adam & Smith (1988) reported  $k_e = 1 \times 10^{-7} \text{ cm}^3 \text{ s}^{-1}$  at 300 K for  $\text{H}_2\text{F}^+ + e$  by a flowing afterglow/Langmuir probe method. This value is seven times smaller than the value calculated from Equations (1) and (2) at 300 K. Nowadays storage ring experiments are well applied for measurements of dissociative recombination rate constants, such as those of  $\text{H}_3^+$  (McCall et al. 2004) and  $\text{HCl}^+$  (Novotny et al. 2013). The method has an advantage in measurement of the temperature dependence of the reaction rate. Neufeld et al. (2012) assumed the following  $k_e$  value of  $\text{H}_2\text{Cl}^+$ , where storage ring data were cited as a private communication:

$$\text{H}_2\text{Cl}^+ + e \rightarrow \text{Cl} + \text{products}$$

$$k_e = 1.2 \times 10^{-7} (T/300 \text{ K})^{-0.85} \text{ cm}^3 \text{ s}^{-1}. \quad (3)$$

At 50 K (approximately the kinetic temperature of low-density clouds), Equations (1) and (2) give  $k_e = 1.7 \times 10^{-6} \text{ cm}^3 \text{ s}^{-1}$  for  $\text{H}_2\text{F}^+$ , and Equation (3) gives  $k_e = 5.5 \times 10^{-7} \text{ cm}^3 \text{ s}^{-1}$  for  $\text{H}_2\text{Cl}^+$ , which is about 1/3 of that of  $\text{H}_2\text{F}^+$ . To check the difference in the recombination rate constants, the present paper reports measurements of the rate constants for the reactions of  $\text{H}_2\text{F}^+$  and  $\text{H}_2\text{Cl}^+$  ions with electrons by using an infrared OPO (optical parametric oscillator) laser coupled with a time-resolved method. Previously, the method of time-resolved infrared laser absorption has been applied to determine the rate constants of  $\text{H}_3^+$ ,  $\text{HCO}^+$ , and  $\text{HN}_2^+$  by Amano (1988, 1990). Later it was found that the determined  $k_e$  value for  $\text{H}_3^+$  is close to the value obtained by storage ring experiments (McCall et al. 2004).

## 2. ASTRONOMICAL OBSERVATIONS

### 2.1. ALMA Observations

We obtained ALMA Cycle 2 observations of the  $\text{H}_2\text{F}^+ 1_{10}-1_{01}$  transition (rest frequency of 760.929 GHz, redshifted to 403.5 GHz, i.e., in ALMA band 8) and HF  $J = 1-0$  transition (rest frequency of 1232.4762 GHz, redshifted to 653.5 GHz, i.e., in ALMA band 9) on 2015 May 14 and May 19, respectively. We adopt a redshift of  $z_{\text{abs}} = 0.88582$ , helio-centric frame, giving  $v = 0 \text{ km s}^{-1}$  for the absorption toward the SW image of PKS 1830–211.

The ALMA correlator was configured with four different spectral windows of 1.875 GHz, each counting 960 channels separated by 1.938 MHz, providing velocity resolutions of  $\sim 1.4$  and  $0.9 \text{ km s}^{-1}$  after Hanning smoothing, in bands 8 and 9, respectively. The spectral windows were centered at  $\sim 401.5$ , 403.5, 413.8, and 415.5 GHz in band 8, and  $\sim 648.0$ , 649.9, 651.7, and 653.6 GHz in band 9. In band 8, we also observed the ortho- $\text{H}_2\text{Cl}^+ 2_{12}-1_{01}$  line (rest frequency of 781.6 GHz). No other lines were detected in the frequency coverage of band 9.

The data calibration was done within the CASA<sup>7</sup> package, following a standard procedure. The bandpass response of the antennas was calibrated from observations of the bright quasar J1924–292. The complex gain solutions were determined by self-calibration of the visibilities of PKS 1830–211, using a simple model of two point sources at the positions of the two lensed images of the blazar. Using a Clean deconvolution (with Briggs weighting and robust parameter set to 0.5), we obtained synthesized beams of  $0''.39 \times 0''.29$  (position angle  $\text{PA} = -84^\circ$ ) in band 8 and  $0''.21 \times 0''.19$  ( $\text{PA} = 64^\circ$ ) in band 9. The two lensed images of PKS 1830–211, separated by  $\sim 1''$ , were spatially well resolved. The spectra were extracted toward both images using the CASA-python task UVMULTIFIT (Martí-Vidal et al. 2014) to fit a model of two point sources to the visibilities.

### 2.2. Herschel Observations

On 2013 February 26–March 7, the  $\text{H}_2\text{F}^+$  ion was searched for toward four sources, W31C (star-forming region,  $\alpha_{2000}: 18^\circ 10'28''.70$ ,  $\beta_{2000}: -19^\circ 55'50''.00$ ), NGC 6334 I (high-mass star-forming region,  $\alpha_{2000}: 17^\circ 20'53''.32$ ,  $\beta_{2000}: -35^\circ 46'58''.5$ ), GC IRS 21 ( $\alpha_{2000}: 17^\circ 45'40''.20$ ,  $\beta_{2000}: -29^\circ 0'31''.00$ ), and 2Mass J17470898-2829561 (J1747) ( $\alpha_{2000}: 17^\circ 47'8''.980$ ,  $\beta_{2000}: -28^\circ 29'56''.10$ ), where the former two sources are known to have abundant HF and  $\text{H}_2\text{Cl}^+$ . In the latter two sources near the Galactic center, the  $\text{H}_3^+$  ion has been detected strongly by infrared observations (Goto et al. 2008, 2011). We searched for two transitions,  $J_{\text{KaKc}} = 2_{12}-1_{01}$  (1850.082 GHz) and  $1_{10}-1_{01}$  (760.929 GHz), from the lowest energy state of ortho levels. We used the dual-beam switch mode and the wideband spectrometer of the *Herschel*/HIFI spectrograph with a spectral resolution of 1.1 MHz ( $\Delta v = 0.43 \text{ km s}^{-1}$  at 760 GHz). The observed data of level 2 were provided as calibrated DSB spectra. The integration time was 8 minutes for each source in the 761 GHz region, and 34 minutes for W31C, 43 minutes for NGC 6334 I, 33 minutes for GC IRS 21, and 31 minutes for 2 Mass J1747 in the 1850 GHz region. The frequency region of the  $1_{11}-0_{00}$  line from the para ground state was not covered by *Herschel*/HIFI because of a lack of the detector system in the

<sup>7</sup> <http://casa.nrao.edu/>

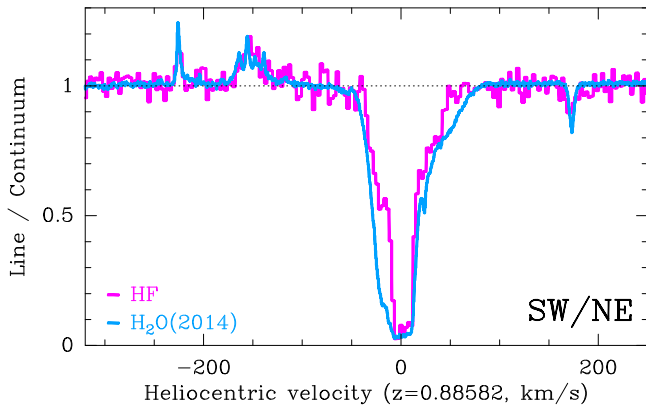


**Figure 1.** Spectrum of the HF  $J = 1-0$  line. Data were smoothed to a velocity resolution of  $2.8 \text{ km s}^{-1}$ . The normalized spectrum toward the SW image has been divided by that toward the NE image in order to remove small bandpass residuals. The SW and NE absorptions appear as features  $<1$  and  $>1$ , respectively. The normalized spectrum of the ground-state transition of ortho- $\text{H}_2\text{O}$   $1_{10}-1_{01}$ , observed in 2014 July, is shown for comparison. The velocity scale is referenced to the heliocentric frame taking  $z = 0.88582$ .

region. The HF  $J = 1-0$  transition at  $1232.47 \text{ GHz}$  was also observed toward NGC 6334 I and two sources near the Galactic center with an integration time of 7 minutes.

### 3. LABORATORY EXPERIMENTS FOR DISSOCIATIVE RECOMBINATIONS OF $\text{H}_2\text{F}^+$ AND $\text{H}_2\text{Cl}^+$

A continuous-wave OPO laser with a spectral width of about  $0.8 \text{ MHz}$  was used to cover the  $3 \mu\text{m}$  infrared region in the present experiment (Okabayashi et al. 2015). It has a bow-tie-type cavity, and a PPLN crystal is pumped by a fiber laser (iPG Photonics YAR-25 K-LP-SF), which is seeded by a DFB laser (Koheras Y10-PM). The output of the OPO laser in the  $3 \mu\text{m}$  region was  $70 \text{ mW}$  for a pumping power of the fiber laser of  $6-8 \text{ W}$ . The  $\text{H}_2\text{F}^+$  ion was produced by a pulsed hollow-cathode discharge in a mixture of  $5\% \text{ F}_2/\text{He}$  and  $\text{H}_2$  gas with partial pressures of  $70 \text{ mTorr}$  ( $9.3 \text{ Pa}$ ) and  $330 \text{ mTorr}$  ( $44 \text{ Pa}$ ), respectively. A high-voltage transistor switch HTS 81 (Behlke Electronic GmbH) was used for the pulsed discharge with peak current of  $200 \text{ mA}$ . In the case of  $\text{H}_2\text{Cl}^+$ , a mixture of  $\text{HCl}$  and  $\text{H}_2$  was used with partial pressures of  $50 \text{ mTorr}$  ( $6.6 \text{ Pa}$ ) and  $330 \text{ mTorr}$  ( $44 \text{ Pa}$ ). The same absorption measurement system was used as in a previous Fourier-transform infrared (FTIR) study of  $\text{H}_2\text{F}^+$  (Fujimori et al. 2013) to attain an effective path length of  $40 \text{ m}$  with a multipath cell arrangement. The glass part of the cell had an inner diameter of  $94 \text{ mm}$  and a length of  $1 \text{ m}$  for the hollow-cathode discharge, and was connected to two glass tubes of inner diameter  $144 \text{ mm}$  and length of  $250 \text{ mm}$  on both sides, keeping a mirror separation of  $150 \text{ cm}$ . The cathode was made of a stainless plate of thickness  $0.1 \text{ mm}$  and mounted on the inner part of the glass cell. The discharge part was cooled by dry-ice. The transmitted laser beam was detected by an infrared mercury-cadmium-telluride detector (Vigo PVI-3TE-4, time constant of  $20 \text{ ns}$ ) followed by a preamplifier (MIPDC-F-100, bandwidth of  $\text{DC}-100 \text{ MHz}$ ).

## 4. RESULTS

### 4.1. ALMA Observations of the $z = 0.89$ Absorber Toward PKS 1830–211

Figure 1 shows the observed absorption due to the HF  $J = 1-0$  transition toward PKS 1830–211. Toward the

southwest (SW) image, the absorption spans a velocity range between about  $-50$  and  $+50 \text{ km s}^{-1}$  and is heavily saturated near  $v = 0 \text{ km s}^{-1}$ . Toward the northeast (NE) image, the absorption covers a velocity range between about  $-250$  and  $-100 \text{ km s}^{-1}$  and reaches at most  $\sim 20\%$  of the continuum level. For comparison, we also show in Figure 1 the absorption spectrum of the ground-state transition of ortho-water, obtained in 2014 April with ALMA. The profiles are nearly identical along the NE line of sight, but the HF absorption has narrower wings than  $\text{H}_2\text{O}$  toward the SW image. Note, however, that time variations of the absorption profiles, with a timescale of months to years, have been observed in this absorber (Muller & Guélin 2008; Muller et al. 2014b) and somewhat limit the direct comparison of spectra taken at different epochs.

Assuming that all HF molecules are in the ground state of  $J = 0$ , the column density is obtained by using the following formula:

$$N_{\text{HF}} = \frac{8\pi^{3/2} \times \Delta v}{2\sqrt{\ln 2} \times \lambda^3 \times A g_u} \times \tau \quad (4)$$

where  $\lambda$  is the wavelength ( $243.2 \mu\text{m}$ ),  $A$  the Einstein A-coefficient ( $2.422 \times 10^{-2} \text{ s}^{-1}$ ), and  $g_l$  and  $g_u$  are the statistical weights of the lower and upper states.  $\tau$  is the optical depth and is given by

$$\tau = -\ln\left(\frac{T_{\text{MB}}}{T_{\text{back}}}\right), \quad (5)$$

where  $T_{\text{MB}}$  and  $T_{\text{back}}$  are the measured brightness temperature and the background continuum temperature, respectively. In the SW direction, by using the linewidth of  $20 \text{ km s}^{-1}$ , the lower limit of  $\tau$  is estimated to be 4 from a simulation of the shape of the absorption line. On the other hand, the  $\tau$  value of NE is obtained to be 0.21. The column densities are determined to be

$$N_{\text{HF}}(\text{SW}) > 3.4 \times 10^{14} \text{ cm}^{-2} \quad [\text{HF}]/[\text{H}_2] > 1.7 \times 10^{-8}$$

$$N_{\text{HF}}(\text{NE}) = 0.18 \times 10^{14} \text{ cm}^{-2} \quad [\text{HF}]/[\text{H}_2] = 1.8 \times 10^{-8}$$

where the abundance relative to  $\text{H}_2$  is calculated by assuming an  $\text{H}_2$  column density of  $\sim 2 \times 10^{22} \text{ cm}^{-2}$  in SW and  $\sim 1 \times 10^{21} \text{ cm}^{-2}$  in NE (Muller et al. 2014b). In the Milky Way, the relative abundance of HF is reported to be  $2.5 \times 10^{-8}$  in NGC 6334 I and  $1.5 \times 10^{-8}$  in AFGL 2591 (Emprechtinger et al. 2012),  $0.8 \times 10^{-8}$  in IRC+10216 (Agúndez et al. 2011),  $(1.1-1.6) \times 10^{-8}$  in W51 and W49N (Sonnentrucker et al. 2010), a conservative lower limit of  $0.6 \times 10^{-8}$  in W31C (Neufeld et al. 2010), and  $1.6 \times 10^{-10}$  in the Orion hot core (Phillips et al. 2010). Sonnentrucker et al. (2015) estimated the HF abundance in Galactic diffuse clouds by using a modified chemical reaction model and found  $[\text{HF}]/[\text{H}_2] = (0.9-3.3) \times 10^{-8}$ , which is consistent with the observed values including those of 12 newly observed sources. The currently obtained abundance in the  $z = 0.89$  absorber is thus close to the values of low-density Galactic clouds.

The redshifted  $403 \text{ GHz}$  region for the  $\text{H}_2\text{F}^+$   $1_{10}-1_{01}$  transition was observed, as shown in Figure 2. The absorption due to  $\text{H}_2\text{F}^+$  is not found, and the rms noise level ( $1\sigma$ ) is estimated to be  $0.5\%$  with  $4.2 \text{ km s}^{-1}$  channels. The absorption occurs from the lowest rotational level of the ortho  $\text{H}_2\text{F}^+$  level, and the second lowest level  $1_{10}$  is located at an energy  $37 \text{ K}$



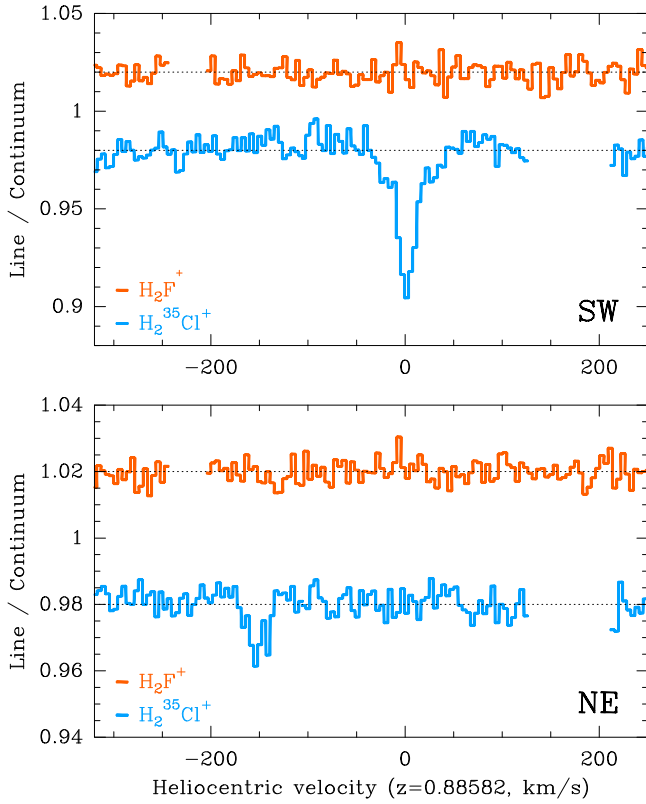


**Figure 2.** Spectra of the  $\text{H}_2\text{F}^+$   $1_{10}-1_{01}$  and  $\text{H}_2\text{Cl}^+$   $2_{12}-1_{01}$  lines, toward the SW image (top) and NE image (bottom), observed simultaneously in the same tuning. Data were smoothed to a velocity resolution of  $4.2 \text{ km s}^{-1}$ . Regions with atmospheric lines were flagged. The velocity scale is referenced to the heliocentric frame taking  $z = 0.88582$ .

higher than the  $1_{01}$  level. Since the  $\text{H}_2$  density of the absorbing gas is relatively low (a few  $10^3 \text{ cm}^{-3}$ ), the excitation of polar species is coupled to the photons of the cosmic microwave background (CMB), with  $T_{\text{CMB}} = 5.14 \text{ K}$  at  $z = 0.89$  (see Muller et al. 2013). We assume that all ortho state molecules are present in the lowest  $1_{01}$  state. By using Equations (4) and (5), we derive the upper limit ( $3\sigma$ ) for the ortho state of the ion to be

$$N_{\text{H}_2\text{F}^+}(\text{SW}) = 6.6 \times 10^{11} \text{ cm}^{-2}$$

where the  $A$ -coefficient is  $0.0200 \text{ s}^{-1}$  and  $\lambda$  is  $394 \mu\text{m}$  for the  $1_{10}-1_{01}$  transition, and we assumed a velocity width of  $20 \text{ km s}^{-1}$ . Table 1 lists the upper limit for the total abundance, including the para state population by assuming an ortho-to-para ratio of 3. It is known that some molecules with ortho-to-para ratios smaller than 3 have been detected, and such molecules are thought to be produced on the surface of low-temperature dust or grains. Some molecules produced by ion-molecule reactions in the gas phase have ratios smaller than 3 (Takakuwa et al. 2001; Morisawa et al. 2006; Faure et al. 2013), originating from abundant para- $\text{H}_2$  in cold clouds. However, in the case of  $\text{H}_2\text{Cl}^+$ , ratios very different from 3 have not been reported (Neufeld et al. 2015), so the assumption of the high-temperature limit value may be valid for  $\text{H}_2\text{Cl}^+$  and also  $\text{H}_2\text{F}^+$ . It is found that the abundance of  $\text{H}_2\text{F}^+$  is less than  $1/386$  of that of HF.

In the same line of sight, Muller et al. (2014a) reported a column density of  $\text{H}_2\text{Cl}^+$  of  $\sim 1.4 \times 10^{13} \text{ cm}^{-2}$  from the

**Table 1**  
Abundances of  $\text{H}_2\text{F}^+$ ,  $\text{H}_2\text{Cl}^+$ , HF, HCl, and  $\text{H}_2$  (Column Density ( $\text{cm}^{-2}$ ))

Species	PKS 1830–211 <sup>a</sup>	W31C	NGC 6334 I
$\text{H}_2\text{F}^+$	$\lesssim 8.8 \times 10^{11}$	$\lesssim 8.1 \times 10^{11}$	$\lesssim 2.5 \times 10^{11}$
$\text{H}_2\text{Cl}^+$	$\sim 1.4 \times 10^{13}$ , <sup>b</sup>	$3.0 \times 10^{13}$ , <sup>c</sup>	$1.7 \times 10^{13}$ , <sup>d</sup>
HF	$> 3.4 \times 10^{14}$	$1.6 \times 10^{14}$ , <sup>e</sup>	$(0.4-2.4) \times 10^{13}$ , <sup>f</sup>
HCl	$3.4 \times 10^{13}$ , <sup>g</sup>	$\sim 2 \times 10^{13}$ , <sup>h</sup>	$1.9 \times 10^{14}$ , <sup>i</sup>
$\text{H}_2$	$\sim 2 \times 10^{22}$ , <sup>j</sup>	$1.2 \times 10^{22}$ , <sup>k</sup>	$(0.6-1.8) \times 10^{21}$ , <sup>f</sup>

**Notes.**

<sup>a</sup> SW line of sight.

<sup>b</sup> Muller et al. (2014a).

<sup>c</sup> Neufeld et al. (2012).

<sup>d</sup> Lis et al. (2010).

<sup>e</sup> Neufeld et al. (2010).

<sup>f</sup> In the foreground components (Emprechtinger et al. 2012).

<sup>g</sup> S. Muller et al. (2016, in preparation).

<sup>h</sup> Monje et al. (2013).

<sup>i</sup>  $T_{\text{ex}} = 39 \text{ K}$  component (Zernickel et al. 2012).

<sup>j</sup> Muller et al. (2011).

<sup>k</sup>  $\text{H}_1$  abundance (Godard et al. 2010).

observation of the para transition  $1_{11}-0_{00}$  and by assuming an ortho-to-para ratio of 3. In the present observation, the ortho transition  $2_{12}-1_{01}$  was detected, as shown in Figure 2. The integrated intensity (opacity) has been obtained as  $2.03 \text{ km s}^{-1}$  and  $0.71 \text{ km s}^{-1}$  toward SW and NE, respectively, and the column density of the ortho ions is estimated to be  $9.1 \times 10^{12} \text{ cm}^{-2}$  and  $3.2 \times 10^{12} \text{ cm}^{-2}$  by assuming that all ortho ions are in the lowest rotational  $1_{01}$  level. The ortho-to-para ratio is 2.7 and 3 in SW and NE, respectively, which are consistent with the high-temperature limit value. Time variations of the absorption profiles (Muller & Guélin 2008) might affect this measurement of the ortho-to-para ratio for  $\text{H}_2\text{Cl}^+$ . Observations close in time would allow us to obtain a very robust ortho-to-para ratio in the two independent lines of sight. The  $\text{H}_2\text{F}^+$  abundance is found to be less than  $1/16$  of that of  $\text{H}_2\text{Cl}^+$ .

#### 4.2. Herschel Observations of Galactic Clouds: Search for Interstellar $\text{H}_2\text{F}^+$

The HF  $J = 1-0$  spectral line was detected toward NGC 6334 I with many saturated absorption components, as reported by Emprechtinger et al. (2012). Spectra observed toward W31C and NGC 6334 I in the 760 GHz region are shown in Figure 3. In the two Galactic center sources GC IRS 21 and 2Mass J1747, no emission and absorption lines have been detected, where the background continuum level was 0.1 K and 0.03 K, respectively. The low continuum levels compared with  $3\sigma$  noise levels of 0.1 K in both objects make it difficult to detect absorption lines. Many emission lines have been detected in W31C and NGC 6334 I, and assignments and analyses of these spectral lines will be reported in a separate paper. The  $\text{H}_2\text{F}^+$  line is expected to be observed as absorption, because the ion is thought to be present in low-density clouds as  $\text{H}_2\text{Cl}^+$ , which is observed as absorption. Toward W31C and NGC 6334 I there was no feature of an absorption line in the 760 GHz region, as shown in Figure 3. In the 1850 GHz region, the noise level was 10–18 times larger than that in the 760 GHz region, so the sensitivity was not enough to detect the  $\text{H}_2\text{F}^+$  line. We estimated the upper limit for the column density to be  $1.9 \times 10^{11} \text{ cm}^{-2}$  in the ortho state toward NGC 6334 I, where we used three times (0.080 K) the rms noise and assumed a

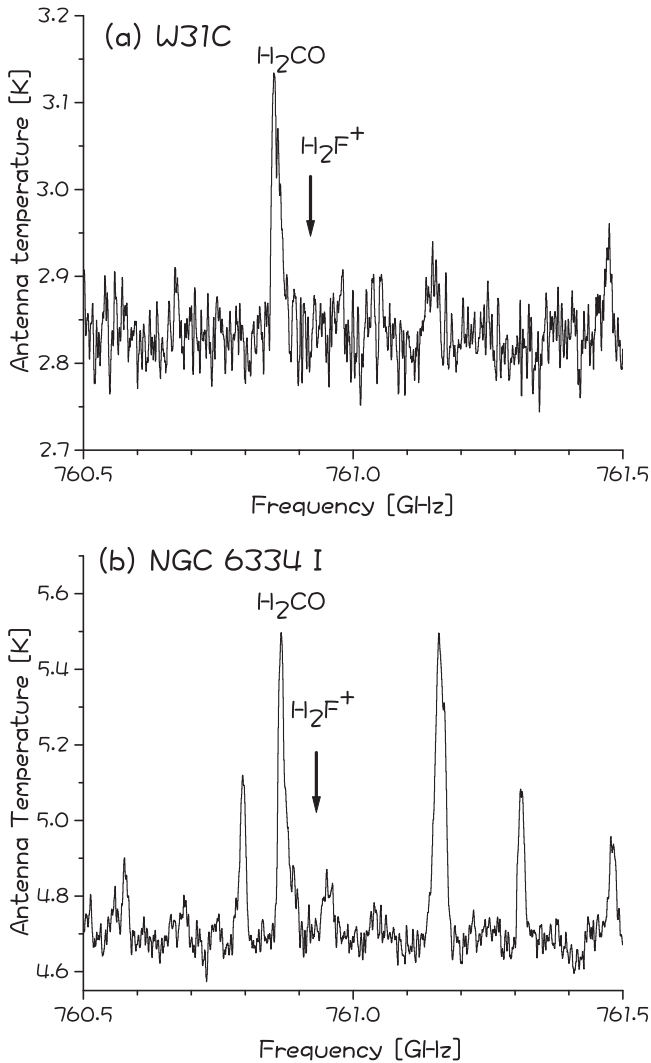


**Figure 3.** Search for the  $\text{H}_2\text{F}^+$   $1_{10}-1_{01}$  spectral line toward W31C and NGC 6334 I, where the frequency scale is given by using the systemic velocities of  $-3 \text{ km s}^{-1}$  and  $-1.7 \text{ km s}^{-1}$ , respectively. The  $\text{H}_2\text{CO}$  line ( $J_{\text{KaKc}} = 10_{19}-9_{18}$ ) is observed in the lower side band at 749.0721 GHz.

velocity width of  $4.93 \text{ km s}^{-1}$ . Similarly, the upper limit toward W31C was estimated by using  $3\sigma = 0.090 \text{ K}$  and assuming a width of  $9.5 \text{ km s}^{-1}$ . The width corresponds to one velocity component among three or four components in the foreground gas of W31C. Table 1 lists total abundances, including the para state population of  $\text{H}_2\text{F}^+$  and related species. Since the abundance of  $\text{H}_2\text{Cl}^+$  has been reported to be  $1.7 \times 10^{13} \text{ cm}^{-2}$  (Lis et al. 2010), which is 4.3% of that of HCl ( $4 \times 10^{14} \text{ cm}^{-2}$ ) in NGC 6334 I, the abundance of  $\text{H}_2\text{F}^+$  is found to be  $1/68$  of that of  $\text{H}_2\text{Cl}^+$ . The solar abundance ratio of F and Cl is reported to be  $804/5170 \sim 1/6$  (Lodders et al. 2009) in the solar photosphere, although an old value of  $1/2$  is quoted in our previous paper (Fujimori et al. 2011). The small abundance of  $\text{H}_2\text{F}^+$  compared with the cosmic atomic abundance may be explained by differences in production and/or depletion mechanisms.

#### 4.3. Laboratory Time-resolved Infrared Laser Spectroscopy of $\text{H}_2\text{F}^+$ and $\text{H}_2\text{Cl}^+$

Figure 4 shows the observed time-resolved spectrum of the  $\text{H}_2\text{F}^+ \nu_3$  band,  $J_{\text{KaKc}} = 3_{13} \leftarrow 4_{14}$  transition at  $3251.99 \text{ cm}^{-1}$

(Fujimori et al. 2013). We also measured the time profile for the  $\text{H}_2\text{Cl}^+ \nu_3$ ,  $J_{\text{KaKc}} = 6_{06} \leftarrow 5_{05}$  and  $6_{16} \leftarrow 5_{15}$  transitions at  $2691.24 \text{ cm}^{-1}$  (Lee et al. 1988), as shown in Figure 5. The time profile shows a rise in absorption due to the ion at the beginning of the pulsed discharge, and after turning off the discharge the absorption intensity of the ion signal decreases with a half-life of a few tens of microseconds. The rotational relaxation time of the ground state is expected to be less than  $1 \mu\text{s}$ , when we assume a pressure-broadening coefficient of  $10\text{--}20 \text{ MHz Torr}^{-1}$ . Therefore, the observed decay is thought to be due to the recombination reaction with an electron. There are many species in the discharge in addition to the reactant  $\text{F}_2$ , He, and  $\text{H}_2$  species. If a product species with a larger proton affinity than HF is present, the proton of  $\text{H}_2\text{F}^+$  moves to the species, and the decay of  $\text{H}_2\text{F}^+$  will be affected compared with the case of just the recombination reaction with an electron. However, the proton transfer occurs at the Langevin rate ( $\sim 10^{-9} \text{ cm}^3 \text{ s}^{-1}$ ), which is two orders of magnitude smaller than the rate of the recombination reaction. Among reactants and products in the discharge, F,  $\text{F}_2$ , He, H, and  $\text{H}_2$  have smaller proton affinities than HF. On the other hand, HF dimer and trimer are thought to have larger proton affinities than HF. However, the spectra of these species were not observed by FTIR (Fujimori et al. 2013) in the same discharge condition, indicating much smaller abundances than HF. So the effects of proton transfer reactions will be neglected in the analysis of the decay of  $\text{H}_2\text{F}^+$ .

In a reaction  $\text{N}^+ + \text{e}^- \rightarrow \text{products}$ , the time variation of the ion density is expressed as follows:

$$-\frac{d[\text{N}^+]}{dt} = k_e[\text{N}^+][\text{e}^-]. \quad (6)$$

When the density of positive ions is equal to that of electrons, the following relation is attained (the second-order reaction scheme):

$$\frac{1}{[\text{N}^+(t)]} = k_e \times t + \frac{1}{[\text{N}^+(0)]}. \quad (7)$$

In the case of  $\text{H}_3^+$ , Amano (1988) could explain the observed decay by Equation (7). On the other hand, the observed decay of  $\text{H}_2\text{F}^+$  of Figure 4(a) was not fitted to the formula of Equation (7) as shown in Figure 4(b), and the decay was found to be fitted to an exponential function as shown in Figure 4(c). This indicates that the reaction proceeds in the pseudo-first-order scheme. That is, by assuming  $[\text{e}^-] \gg [\text{N}^+(t)]$ ,

$$\ln[\text{N}^+(t)] = -k_e[\text{e}^-]t + \ln[\text{N}^+(0)] \quad (8)$$

where  $[\text{N}^+(0)]$  is the abundance at the starting time of decay  $t = 0$ . For  $\text{H}_2\text{Cl}^+$ , the same exponential fitting as  $\text{H}_2\text{F}^+$  was found to be better. In the first-order reaction scheme, the electron density is higher than that of  $\text{H}_2\text{F}^+$  or  $\text{H}_2\text{Cl}^+$ . For neutrality of the discharge plasma producing  $\text{H}_2\text{F}^+$ , other positive ions should carry the positive charge. Although positive ions such as  $\text{F}_2^+$ ,  $\text{F}^+$ ,  $\text{H}^+$ ,  $\text{He}^+$ , and protonated  $(\text{HF})_2$  will be candidates, we did not monitor these species in the present experiment. In a pure hydrogen discharge, the  $\text{H}_3^+$  ion was observed by FTIR (Fujimori et al. 2013), but the spectrum disappeared when the  $\text{F}_2/\text{He}$  gas mixture was added to the discharge. In the present discharge, the  $\text{H}_2\text{F}^+$  ion is thought to be produced by reactions  $\text{H}_2^+ + \text{HF}$  and  $\text{HF}^+ + \text{H}_2$ , where we monitored the HF absorption with FTIR. The  $\text{HF}^+$  ion was observed by laser

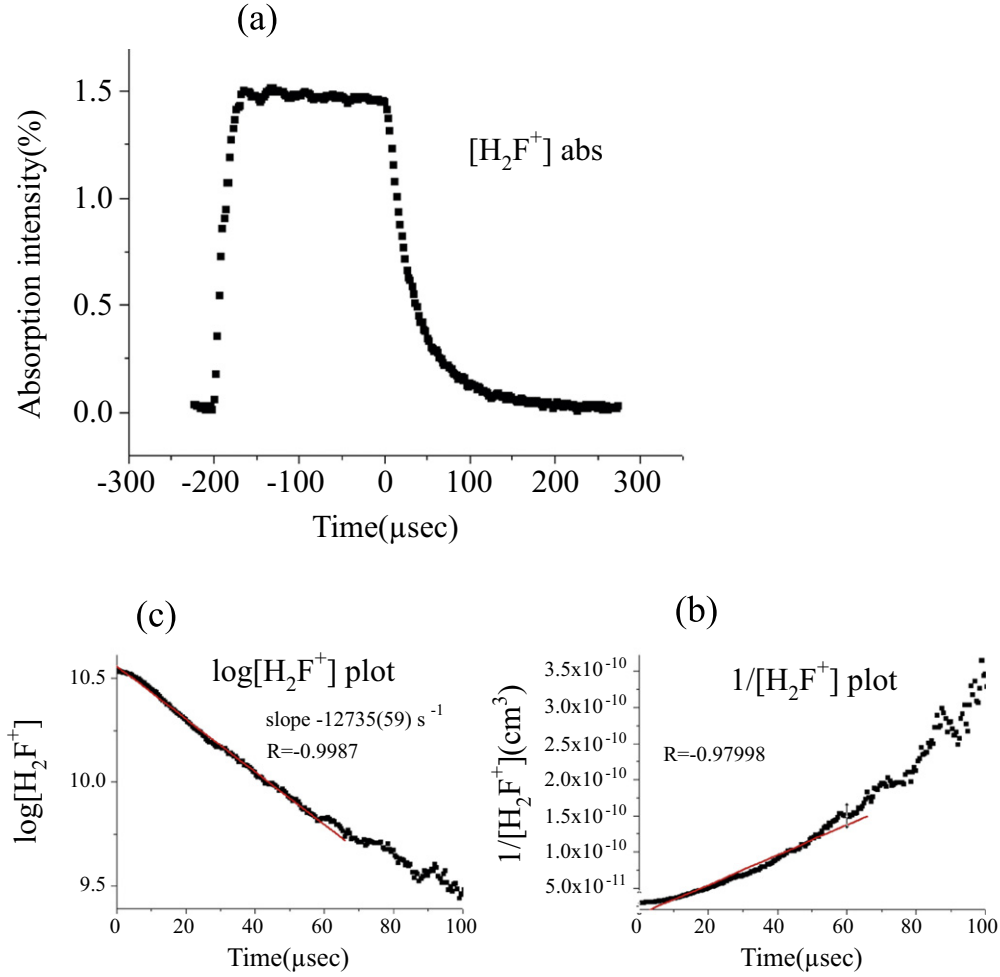


**Figure 4.** (a) Time-resolved spectrum of the  $\text{H}_2\text{F}^+\nu_3$  band,  $J_{\text{KaKc}} = 3_{13} \leftarrow 4_{14}$  transition at  $3251.99 \text{ cm}^{-1}$  obtained by a pulsed discharge with peak current of 200 mA, (b)  $1/N$  fit, (c) exponential fit.

spectroscopy (Hovde et al. 1989) in a discharge of a mixture of a large amount of He and HF. In the present condition, the ion was not observed with FTIR in the  $3.3 \mu\text{m}$  region, because of rapid reaction with  $\text{H}_2$ .

By least-squares fittings of the observed decay curves, we determined the  $k_e[\text{e}^-]$  values for  $\text{H}_2\text{F}^+$  and  $\text{H}_2\text{Cl}^+$ , as shown in Figure 6, where the error bars correspond to the range of several measurements at a constant value of current. As is known in a glow discharge (Teii 1986), Figure 6 shows that the electron density is proportional to the discharge current. To determine  $k_e$ , we have to obtain the electron density  $[\text{e}^-]$ , so we utilized a method with a single Langmuir probe (von Engel 1983; Teii 1986). When we set a discharge in a mixture of 9.3 Pa  $\text{F}_2/\text{H}_2$  and 44 Pa  $\text{H}_2$  with a DC current of 200 mA at the probe position between two electrodes, the density was obtained to be  $(2.65\text{--}2.85) \times 10^{11} \text{ electrons cm}^{-3}$ . In the case of a pure hydrogen discharge ( $\text{H}_3^+$  production), a density of  $(2.55\text{--}2.75) \times 10^{11} \text{ electrons cm}^{-3}$  was obtained. Since the difference in the density between conditions producing  $\text{H}_3^+$  and  $\text{H}_2\text{F}^+$  was small, we assumed the same density for the production of  $\text{H}_2\text{Cl}^+$ . By averaging three measurements, we obtained  $[\text{e}^-] = (2.78 \pm 0.56) \times 10^{11} \text{ cm}^{-3}$ , where the error corresponds to the range of the observed values.

We also derived the ion density at  $t = 0$  for comparison with the electron density, although the value is not necessary for

deriving the rate constant in the case of the first-order reaction scheme. The procedure is described by Bernath (2005), and we used the transition moment of 0.322 Debye for the  $\text{H}_2\text{F}^+\nu_3$  band, reported by Bunker et al. (1990). The rotational temperature was fixed at the value of 209 K determined from Fourier-transform absorption spectroscopy of  $\text{H}_3^+$  (Fujimori et al. 2013). The partition function was calculated numerically from the lowest energy level, until the new value does not contribute to 1% of the summed total value. The estimated abundance of  $\text{H}_2\text{F}^+$  is  $(3.3 \pm 0.7) \times 10^{10} \text{ cm}^{-3}$ , where we confirmed that the ion density is an order of magnitude smaller than the electron density  $[\text{e}^-]$  in the present experimental condition.

By using the  $k_e[\text{e}^-]$  value of Figure 6 at 200 mA, we obtained the following dissociative recombination rate constants:

$$k_e(\text{H}_2\text{F}^+) = (1.08 \pm 0.29) \times 10^{-7} \text{ cm}^3 \text{ s}^{-1}$$

$$k_e(\text{H}_2\text{Cl}^+) = (0.46 \pm 0.05) \times 10^{-7} \text{ cm}^3 \text{ s}^{-1}.$$

The present value for  $\text{H}_2\text{F}^+$  is in agreement with that obtained by the flowing afterglow experiment, and eight times smaller than the value calculated from Equations (1) and (2) at 209 K. It is noted that in interstellar space the ion is distributed in only the lowest rotational levels of the ortho and para states. On the other

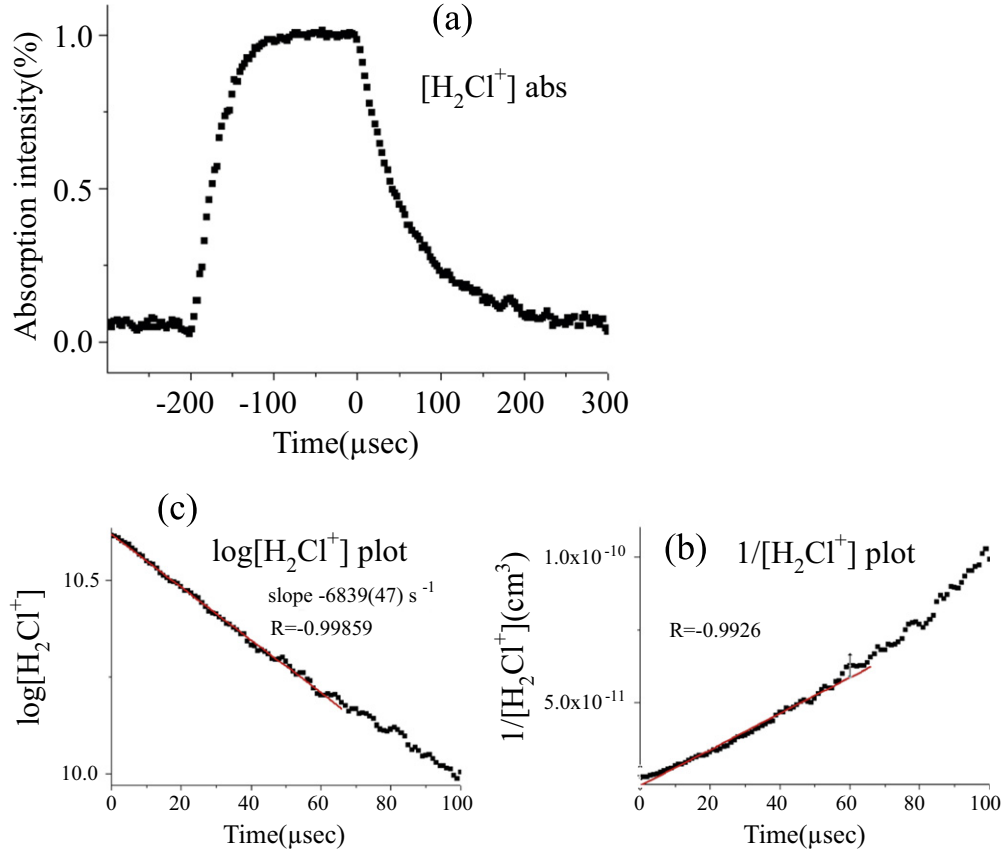


**Figure 5.** (a) Time-resolved spectrum of the  $\text{H}_2\text{Cl}^+\nu_3$  band,  $J_{\text{KaKc}} = 6_{06} \leftarrow 5_{05}$  and  $6_{16} \leftarrow 5_{15}$  transitions at  $2691.24 \text{ cm}^{-1}$  obtained by a pulsed discharge with peak current of 300 mA, (b)  $1/N$  fit, (c) exponential fit.

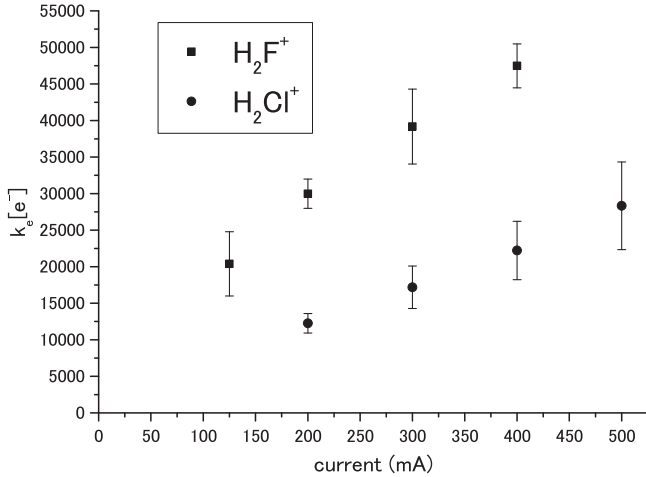


**Figure 6.** Product of the dissociative recombination constant ( $k_e$ ) and electron density  $[e^-]$  obtained by the fittings of decay curves at various values of discharge current.

## 5. DISCUSSION

The  $k_e$  value of  $\text{H}_2\text{F}^+$  has been determined experimentally at 209 K. The present method is not applicable for lower temperatures, because of the adhesion of the reactants on the glass surface. In interstellar diffuse clouds, the translational temperature is expected to be around 50 K, so we estimated the  $k_e$  value by using temperature-dependent terms of Equations (1)–(3) and the present values for the magnitude terms, and found  $k_e(50 \text{ K}) = 2.2(5) \times 10^{-7}$  and  $1.6(4) \times 10^{-7} \text{ cm}^3 \text{ s}^{-1}$  for  $\text{H}_2\text{F}^+$  and  $\text{H}_2\text{Cl}^+$ , respectively. The difference in dissociative recombination rates between  $\text{H}_2\text{F}^+$  and  $\text{H}_2\text{Cl}^+$  is not large. Since the temperature-dependent terms of Equations (1)–(3) have not been confirmed experimentally, there may be ambiguity in the estimation. However, even with the same temperature dependence for both rates, the difference is only a factor of 2.3. Therefore, the observed small interstellar abundance of  $\text{H}_2\text{F}^+$  compared with that of  $\text{H}_2\text{Cl}^+$  is thought to be mainly due to the production mechanism.

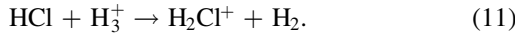
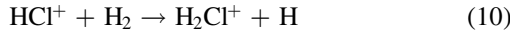
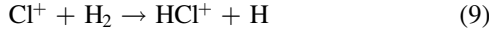
The present value of  $k_e(50 \text{ K})$  for  $\text{H}_2\text{Cl}^+$  is 3.4 times smaller than that derived from Equation (3). This smaller rate increases the abundance of  $\text{H}_2\text{Cl}^+$  and is in better agreement with astronomical observations, where the observed  $\text{H}_2\text{Cl}^+$  ion is reported to be 5–10 times (Neufeld et al. 2012, 2015) more abundant than the estimate in previous chemical models of diffuse clouds.

The ionization potentials of Cl and HCl are smaller than that of hydrogen. On the other hand, F and HF have larger ionization energies than hydrogen. The  $\text{H}_2\text{Cl}^+$  ion is thought to

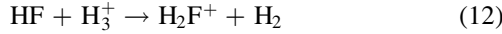
hand, the present laboratory measurement for  $\text{H}_2\text{F}^+$  was carried out for the transition from the seventh lowest energy level of ortho, because of weak intensities of transitions from the lowest  $1_{01}$  level. In the case of  $\text{H}_3^+$  and  $\text{HCO}^+$ , the  $k_e$  values for several rotational states are in agreement within the measurement error limit (Amano 1990). So we assume the same rate for the laboratory and the astronomically observed levels. The  $k_e$  value of  $\text{H}_2\text{Cl}^+$  is half of that given by Equation (3), and a factor 2 larger than that of  $\text{HCl}^+$  at 209 K (Novotny et al. 2013).



be produced via two routes in interstellar space:



In diffuse clouds, the presence of  $\text{HCl}^+$  is important for production of  $\text{H}_2\text{Cl}^+$  by a reaction with  $\text{H}_2$ , and the ion has been detected by *Herschel* HIFI (De Luca et al. 2012). On the other hand, F and HF are not ionized by the interstellar radiation field, although the reaction of  $\text{F}^+$  with  $\text{H}_2$  produces  $\text{HF}^+$ . Therefore, a possible route for  $\text{H}_2\text{F}^+$  production is thought to be



with a formation rate  $k_f(\text{H}_3^+) = 1.2 \times 10^{-8}(T/300 \text{ K})^{-0.15} \text{ cm}^3 \text{ s}^{-1}$  (Neufeld et al. 2005). Recently, the detection of  $\text{CF}^+$  toward PKS 1830–211 (SW) has been reported with a column density of  $5.5 \times 10^{12} \text{ cm}^{-2}$  (Muller et al. 2016). If the reaction of HF and  $\text{C}^+$  is the main route for the production of  $\text{CF}^+$ , the  $\text{CF}^+$  abundance is given in the steady-state approximation as follows:

$$[\text{CF}^+] = \frac{k_f(\text{CF}^+)[\text{HF}][\text{C}^+]}{k_e(\text{CF}^+)[\text{e}^-]} \quad (13)$$

where  $k_f(\text{CF}^+)$  denotes the formation rate of  $\text{CF}^+$  by the reaction  $\text{HF} + \text{C}^+$ , and  $k_e(\text{CF}^+)$  the dissociative recombination rate for  $\text{CF}^+ + \text{e}$ . A similar formula is given for  $\text{H}_2\text{F}^+$ :

$$[\text{H}_2\text{F}^+] = \frac{k_f(\text{H}_2\text{F}^+)[\text{HF}][\text{H}_3^+]}{k_e(\text{H}_2\text{F}^+)[\text{e}^-]}. \quad (14)$$

From Equations (13) and (14) the abundance ratio of  $\text{H}_2\text{F}^+$  and  $\text{CF}^+$  is given as follows:

$$\begin{aligned} \frac{[\text{H}_2\text{F}^+]}{[\text{CF}^+]} &= \frac{k_f(\text{H}_2\text{F}^+)k_e(\text{CF}^+)[\text{H}_3^+]}{k_f(\text{CF}^+)k_e(\text{H}_2\text{F}^+)[\text{C}^+]} \\ &= 1.7 \frac{k_e(\text{CF}^+)[\text{H}_3^+]}{k_e(\text{H}_2\text{F}^+)[\text{C}^+]} = 1.6 \frac{[\text{H}_3^+]}{[\text{C}^+]} \end{aligned} \quad (15)$$

where the last part is obtained by using the present  $k_e(\text{H}_2\text{F}^+)$ . Gerin et al. (2015) reported an abundance ratio  $[\text{C}]/[\text{H}] = (1.5 \pm 0.4) \times 10^{-4}$  in diffuse clouds by *Herschel* observation of  $\text{C}^+$ . The  $[\text{H}_3^+]$  abundance is estimated to be  $\zeta [\text{H}_2]/k_e(\text{H}_3^+)[\text{e}^-]$  (McCall et al. 2002), where  $\zeta$  is the cosmic-ray ionization rate and  $k_e(\text{H}_3^+)$  the dissociative recombination rate constant. Considering the fraction of protons in  $\text{H}_2$  (McCall et al. 2002), when we assume  $\zeta = 2 \times 10^{-16} \text{ s}^{-1}$  (Indriolo et al. 2007),  $k_e(\text{H}_3^+) = 2 \times 10^{-7} \text{ cm}^3 \text{ s}^{-1}$ , and  $[\text{e}^-] = [\text{C}]$ , the  $\text{H}_2\text{F}^+$  abundance is expected to be 3.5% of that of  $\text{CF}^+$ , that is,  $[\text{H}_2\text{F}^+] = 1.9 \times 10^{11} \text{ cm}^{-2}$  toward PKS 1830–211, which is smaller than the present upper limit of  $8.8 \times 10^{11} \text{ cm}^{-2}$ . Non-detection of  $\text{H}_2\text{F}^+$  toward W31C, NGC 6334 I, and PKS 1830–211 may be explained by the low abundance of  $\text{H}_3^+$ . On the other hand, the Galactic center source GC IRS 21 has been reported with a large  $\text{H}_3^+$  column density of  $61.3 \times 10^{14} \text{ cm}^{-2}$  (Goto et al. 2008). However, the continuum level in the 760 GHz region is too low to detect absorption lines of the  $\text{H}_2\text{F}^+$  ion. Only five sources have been observed in the present study, so further searches will be

necessary to detect the  $\text{H}_2\text{F}^+$  ion in sources with high  $\text{H}_3^+$  abundance and a high continuum level.

## 6. SUMMARY

The HF molecule was detected in the  $z = 0.89$  absorber in front of PKS 1830–211 with ALMA, and its abundance relative to  $\text{H}_2$  ( $> 1.7 \times 10^{-8}$ ) is similar to that of other diffuse clouds in the Galaxy, indicating that HF is an excellent tracer of molecular hydrogen even in the interstellar medium of distant galaxies. In spite of the abundant HF, the protonated  $\text{H}_2\text{F}^+$  ion is detected neither toward PKS 1830–211 nor toward a sample of four Galactic sources (W31C, NGC 6334 I, IRS 21, and 2Mass J1747). In contrast, the  $\text{H}_2\text{Cl}^+$  ion is detected with a column density more than an order of magnitude higher than that of  $\text{H}_2\text{F}^+$  in the observed sources. Laboratory experiments on dissociative recombination reactions provide a smaller rate for  $\text{H}_2\text{F}^+$  than the previous prediction.

This paper makes use of the following ALMA data: ADS/JAO.ALMA#2013.1.01099.S. ALMA is a partnership of ESO (representing its member states), NSF (USA), and NINS (Japan), together with NRC (Canada), NSC and ASIAA (Taiwan), and KASI (Republic of Korea), in cooperation with the Republic of Chile. The Joint ALMA Observatory is operated by ESO, AUI/NRAO, and NAOJ.

HIFI has been designed and built by a consortium of institutes and university departments from across Europe, Canada, and the United States under the leadership of SRON Netherlands Institute for Space Research, Groningen, The Netherlands and with major contributions from Germany, France, and the US Consortium members are: Canada: CSA, U. Waterloo; France: CESR, LAB, LERMA, IRAM; Germany: KOSMA, MPIfR, MPS; Ireland, NUI Maynooth; Italy: ASI, IFSI-INAF, Osservatorio Astrofisico di Arcetri-INAF; Netherlands: SRON, TUD; Poland: CAMK, CBK; Spain: Observatorio Astronómico Nacional (IGN), Centro de Astrobiología (CSIC-INTA). Sweden: Chalmers University of Technology—MC2, RSS & GARD; Onsala Space Observatory; Swedish National Space Board, Stockholm University—Stockholm Observatory; Switzerland: ETH Zurich, FHNW; USA: Caltech, JPL, NHSC.

We thank Mina Imai for her contribution to the initial analysis of *Herschel* HIFI data. The present study was partly supported by the Grant-in-Aid from the Ministry of Education, Culture, Sports, Science and Technology of Japan (grant no. 21104003).

## REFERENCES

- Adam, N. G., & Smith, D. 1988, *CPL*, **144**, 11
- Agúndez, M., Cernicharo, J., Waters, L. B., F. M., et al. 2011, *A&A*, **533**, L6
- Amano, T. 1988, *ApJL*, **329**, L121
- Amano, T. 1990, *JChPh*, **92**, 6492
- Amano, T., Matsushima, F., Shiraishi, T., et al. 2012, *JChPh*, **137**, 134308
- Bernath, P. 2005, *Spectra of Atoms and Molecules* (New York: Oxford Univ. Press)
- Bunker, P. R., Jensen, P., Wright, J. S., & Hamilton, I. P. 1990, *JMoSp*, **144**, 310
- Cernicharo, J., & Guélin, M. 1987, *A&A*, **183**, L10
- De Luca, M., Gupta, H., Neufeld, D., et al. 2012, *ApJ*, **751**, 37
- Emprechtinger, M., Monje, R. R., van der Tak, F. F. S., et al. 2012, *ApJ*, **756**, 136
- Faure, A., Hily-Blant, P., Le Gal, R., Rist, C., & Pineau des Forêts, G. 2013, *ApJL*, **770**, L2



- Fujimori, R., Hirata, Y., Morino, I., & Kawaguchi, K. 2013, *JPhCh*, A117, 9882
- Fujimori, R., Kawaguchi, K., & Amnao, T. 2011, *ApJL*, 729, L2
- Geppert, W. D., & Larsson, M. 2008, *MolPh*, 106, 2199
- Gerin, M., Ruaud, M., Goicoechea, J. R., et al. 2015, *A&A*, 573, 30
- Godard, B., Falgarone, E., Gerin, M., Hily-Blant, P., & de Luca, M. 2010, *A&A*, 520, 20
- Goto, M., Usuda, T., Geballe, T. R., et al. 2011, *PASJ*, 63, L13
- Goto, M., Usuda, T., Nagata, T., et al. 2008, *ApJ*, 688, 306
- Hovde, D. C., Keim, E. R., & Saykally, R. J. 1989, *MolPh*, 68, 599
- Indriolo, N., Geballe, T. R., Oka, T., & McCall, B. J. 2007, *ApJ*, 671, 1736
- Lee, S. K., Amano, T., Kawaguchi, K., & Oldani, M. 1988, *JMoSp*, 130, 1
- Lis, D. C., Pearson, J. C., Neufeld, D. A., et al. 2010, *A&A*, 521, L9
- Lodders, K., Palme, H., & Gail, H. P. 2009, *Landolt-Bornstein, New Series, Astronomy and Astrophysics* (Berlin: Springer)
- Martí-Vidal, I., Vlemmings, W., Muller, S., & Casey, S. 2014, *A&A*, 563, 136
- McCall, B. J., Hinkle, K. H., Greballe, T. R., et al. 2002, *ApJ*, 567, 391
- McCall, B. J., Huneycutt, A. J., Saykally, R. J., et al. 2004, *PhRv*, 70, 052716
- Monje, R. R., Emprechtinger, M., Phillips, T. G., et al. 2011a, *ApJL*, 734, L23
- Monje, R. R., Lis, D. C., Roueff, E., et al. 2013, *ApJ*, 767, 81
- Monje, R. R., Lord, S., Falgarone, E., et al. 2014, *ApJ*, 785, 22
- Monje, R. R., Phillips, T. G., Peng, R., et al. 2011b, *ApJ*, 741, 21
- Morisawa, Y., Fushitani, M., Kato, Y., et al. 2006, *ApJ*, 642, 954
- Muller, S., Beelen, A., Black, J. H., et al. 2013, *A&A*, 551, 109
- Muller, S., Beelen, A., Guélin, M., et al. 2011, *A&A*, 535, 103
- Muller, S., Black, J. H., Guelin, M., et al. 2014a, *A&A*, 566, 6
- Muller, S., Combes, F., Guélin, M., et al. 2014b, *A&A*, 566, 112
- Muller, S., & Guélin, M. 2008, *A&A*, 491, 739
- Muller, S., Kawaguchi, K., Black, J. H., & Amano, T. 2016, *A&A*, 566, L5
- Neufeld, D. A., Black, J. H., Gerin, M., et al. 2015, *ApJ*, 807, 54
- Neufeld, D. A., Roueff, E., Snell, R., et al. 2012, *ApJ*, 748, 37
- Neufeld, D. A., Schilke, P., Menten, K. M., et al. 2006, *A&A*, 454, L37
- Neufeld, D. A., Sonnentrucker, P., Phillips, T. G., et al. 2010, *A&A*, 518, L108
- Neufeld, D. A., & Wolfire, M. G. 2009, *ApJ*, 706, 1594
- Neufeld, D. A., Wolfire, M. G., & Schilke, P. 2005, *ApJ*, 628, 260
- Neufeld, D. A., Zmuidzinas, J., Schilke, P., & Phillips, T. G. 1997, *ApJL*, 488, L141
- Novotny, O., Becker, A., Buhr, H., et al. 2013, *ApJ*, 777, 54
- Okabayashi, Y., Miyamoto, Y., Tang, J., & Kawaguchi, K. 2015, *CPL*, 619, 144
- Ossenkopf, V., Müller, H. S. P., Lis, D. C., et al. 2010, *A&A*, 518, L111
- Phillips, T. G., Bergin, E. A., Lis, D. C., et al. 2010, *A&A*, 518, L109
- Plašil, R., Glosik, J., Poterya, V., et al. 2002, *IJMSp*, 218, 105
- Rangwala, N., Maloney, P. R., Glenn, J., et al. 2011, *ApJ*, 743, 94
- Schilke, P., Neufeld, D. A., Müller, H. S. P., et al. 2014, *A&A*, 566, A29
- Sonnentrucker, P., Neufeld, D. A., Phillips, T. G., et al. 2010, *A&A*, 521, L12
- Sonnentrucker, P., Wolfire, M., Neufeld, D. A., et al. 2015, *A&A*, 806, 49
- Takakuwa, S., Kawaguchi, K., Mikami, H., & Saito, M. 2001, *PASJ*, 53, 251
- Teii, S. 1986, *Purazuma Kisokougaku* (Tokyo: Uchida Rokakuho) (in Japanese)
- van der Werf, P. P., Isaak, K. G., Meijeerink, R., et al. 2010, *A&A*, 518, L42
- von Engel, A. 1983, *Electric Plasmas: Their Nature and Uses* (New York: Taylor and Francis)
- Zernickel, A., Schilke, P., Schmiedeke, A., et al. 2012, *A&A*, 546, A87